Acta Crystallographica Section B
Structural Science
ISSN 0108-7681

Single-crystal diffuse scattering studies on polymorphs of molecular crystals. I. The room-temperature polymorphs of the drug benzocaine

E. J. Chan,[a] T. R. Welberry,[a]* D. J. Goossens,[a] A. P. Heerdegen,[a] A. G. Beasley[a] and P. J. Chupas[b]

[a]Research School of Chemistry, Australian National University, Canberra, ACT 0200, Australia, and [b]Advanced Photon Source, Argonne National Laboratory, Argonne, IL, USA

Correspondence e-mail: welberry@rsc.anu.edu.au

Received 12 December 2008
Accepted 28 April 2009

The drug benzocaine (ethyl 4-aminobenzoate), commonly used as a local anaesthetic, is a bimorphic solid at room temperature. Form (I) is monoclinic $P2_1/c$, while the metastable form (II) is orthorhombic $P2_12_12_1$. Three-dimensional diffuse X-ray scattering data have been collected for the two forms on the 11-ID-B beamline at the Advanced Photon Source (APS). Both forms show strong and highly structured diffuse scattering. The data have been interpreted and analysed using Monte Carlo (MC) modelling on the basis that the scattering is purely thermal in origin and indicates the presence of highly correlated molecular motions. In both forms (I) and (II) broad diffuse streaks are observed in the $0kl$ section which indicate strong longitudinal displacement correlations between molecules in the $\langle 031 \rangle$ directions, extending over distances of up to 50 Å. Streaks extending between Bragg peaks in the $hk0$ section normal to [100] correspond to correlated motions of chains of molecules extending along **a** that are linked by N—H···O═C hydrogen bonds and which occur together as coplanar ribbon pairs. The main difference between the two forms is in the dynamical behaviour of the ribbon pairs and in particular how they are able to slide relative to each other. While for form (I) a model involving harmonic springs is able to describe the motion satisfactorily, as simple excursions away from the average structure, there is evidence in form (II) of anharmonic effects that are precursors of a phase transition to a new low-temperature phase, form (III), that was subsequently found.

1. Introduction

Polymorphism refers to the situation where a substance may crystallize in more than one different crystal form. In addition to its scientific interest, polymorphism is a matter of practical and commercial importance in the pharmaceutical and other manufacturing industries (Bernstein, 2002). Crystal form can affect such things as ease of manufacture and processing, shelf-life and, most importantly in the case of pharmaceuticals, the rate of uptake of the molecule by the human body (Knapman, 2000). There is consequently a great need to be able to understand, predict and control polymorphism.

To date efforts to obtain such understanding have relied heavily on the results of conventional crystallography – obtaining the *average* crystal structure using Bragg diffraction data. The present study is part of a research program in which we are using X-ray diffuse scattering methods to investigate the rôle played by molecular flexibility and disorder in the occurrence of polymorphism. Diffuse scattering contains two-body information, which is information over and above the single-body information that is obtainable from Bragg scattering, and this enables the local structure and dynamics to be

Table 1
Cell data for the three polymorphs, (I), (II) and (III), of benzocaine, $C_9H_{11}O_2N$, (BZC).

Polymorph	BZC (I)	BZC (II)	BZC (III)
Space group	$P2_1/c$ (No. 14)	$P2_12_12_1$ (No. 19)	$P2_1$ (No. 4)
a (Å)	8.2570 (2)	8.2424 (9)	8.1883 (4)
b (Å)	5.5009 (4)	5.3111 (3)	10.6374 (5)
c (Å)	19.9560 (2)	20.9044 (2)	20.4761 (1)
α (°)	90.0	90.0	90.0
β (°)	91.699 (4)	90.0	90.0
γ (°)	90.0	90.0	99.370 (2)
V (Å^3)	906.02 (14)	915.12 (9)	1760.05 (15)
Z	4	4	8
Temperature (K)	300	300	150

probed (Beasley *et al.*, 2008). In some instances static (occupational) disorder may feature in these studies, but in others the disorder is of thermal origin and the resulting thermal diffuse scattering (TDS) is used to obtain details of the correlations that occur between both the inter- and intramolecular displacements.

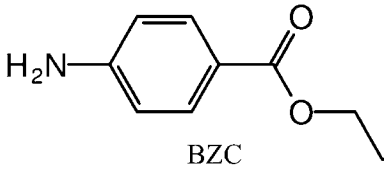

BZC

In the present paper we report on room-temperature studies, using diffuse scattering methods, of the pharmaceutical compound benzocaine or ethyl 4-aminobenzoate, $C_9H_{11}O_2N$, (BZC). BZC is still commonly used as a topical local anaesthetic and in sunscreen. It is made widely available in emulsions and solutions for such purposes. Being a polymorphic pharmaceutical the thermodynamic and kinetic properties of BZC have been subjected to thorough investigation (Gruno *et al.*, 1993; Schmidt, 2005). This and the fact that crystals suitable for diffuse scattering studies can readily be grown make it an ideal compound for this type of study. Room-temperature single-crystal X-ray diffraction studies reveal the existence of two polymorphs for BZC, one crystallizing as monoclinic $P2_1/c$ [polymorph (I); Lynch & McClenaghan, 2002], the other as orthorhombic $P2_12_12_1$ [polymorph (II); Sinha & Pattabhi, 1987]. As a result of the present studies a third low-temperature polymorph [polymorph (III)] has been found. Discussion of the transformation to this polymorph and details of its stucture will be published in subsequent papers. Cell data for the three polymorphs are given in Table 1.

Although the recording and measurement of three dimensional X-ray diffuse scattering data has become relatively routine, the interpretation and analysis of such data is still non-trivial. We have developed a method in which Monte Carlo (MC) simulation of a model crystal is used to analyse the data and this has become a well accepted method by which even the most complex diffuse scattering problems can be tackled (Welberry & Butler, 1994; Welberry, 2004). The advantage of the method is that it can be applied generally to all systems, regardless of their complexity or the size of the atomic displacements that might be present. The only limitation is the extent to which the MC energy can be made to realistically represent the real system energy. On the one hand a very simplified model may be useful in demonstrating particular qualitative effects (Welberry, 2001), while on the other a quantitative and very detailed description of a disordered structure can be obtained (Welberry *et al.*, 2001). With the continued evolution of ever faster and cheaper computers the method continues to improve correspondingly, both in the size of system that can be handled and in the level of detail that can be revealed.

2. Experimental

2.1. Crystal growth

Single crystals of both forms suitable for diffuse scattering experiments were obtained by evaporation of saturated ethanolic solutions at room temperature. Form (I) was a colourless block with dimensions $1.0 \times 2.2 \times 3.5$ mm^3, form (II) was a colourless prism with dimensions $1.0 \times 2.0 \times 3.0$ mm^3.

2.2. Bragg experiment

Details of the Bragg experiments for all forms will be the subject of a subsequent paper (Chan *et al.*, 2009). It should be noted that for ease of structural comparison between the two forms, the atomic coordinates for form (II) were placed in a non-standard setting of $P2_12_12_1$ using the transformation $x, y, z \longrightarrow -y + \frac{1}{4}, x, z + \frac{1}{4}$ giving equivalent positions x, y, z; $-x, y + \frac{1}{2}, -z + \frac{1}{2}$; $x + \frac{1}{2}, -y, -z$; $-x + \frac{1}{2}, -y + \frac{1}{2}, z + \frac{1}{2}$. All written and graphical material in this and future papers, on the subject of the diffuse scattering of BZC, uses this non-standard setting for form (II).

Fig. 1 shows drawings of the structures of forms (I) and (II) of BZC viewed in projection down the principal axes. The intermolecular stacking of the two polymorphs is very similar. In both structures ribbons of molecules involving strong end-on N—H···O hydrogen bonds (blue dotted lines in Figs. 1*a* and *b*) are generated by translations along the *a* axis. Coplanar pairs of these ribbon motifs are interlocked sequentially *via* the in-plane interactions of the ethyl groups (pink dotted lines). These ribbon pairs are identified by the light blue shaded envelopes both in Figs. 1(*a*) and (*b*), and in Figs. 1(*e*) and (*f*). The ribbon pairs are interconnected through quasi-perpendicular N—H···N hydrogen bonds (green solid lines) *via* a 2_1 screw axis along **b** and this generates the herring-bone arrangement of the ribbon pairs when the structure is viewed down the *a* axis (Figs. 1*e* and *f*). The stacking difference between the two polymorphs is simply how the ethyl groups of the two halves of each ribbon-pair slot into each other, *i.e.* these are either related by a 2_1-screw or an inversion centre.

2.3. Diffuse scattering experiment

Three-dimensional X-ray diffuse scattering data were collected at room temperature on the 11-ID-B beamline at the

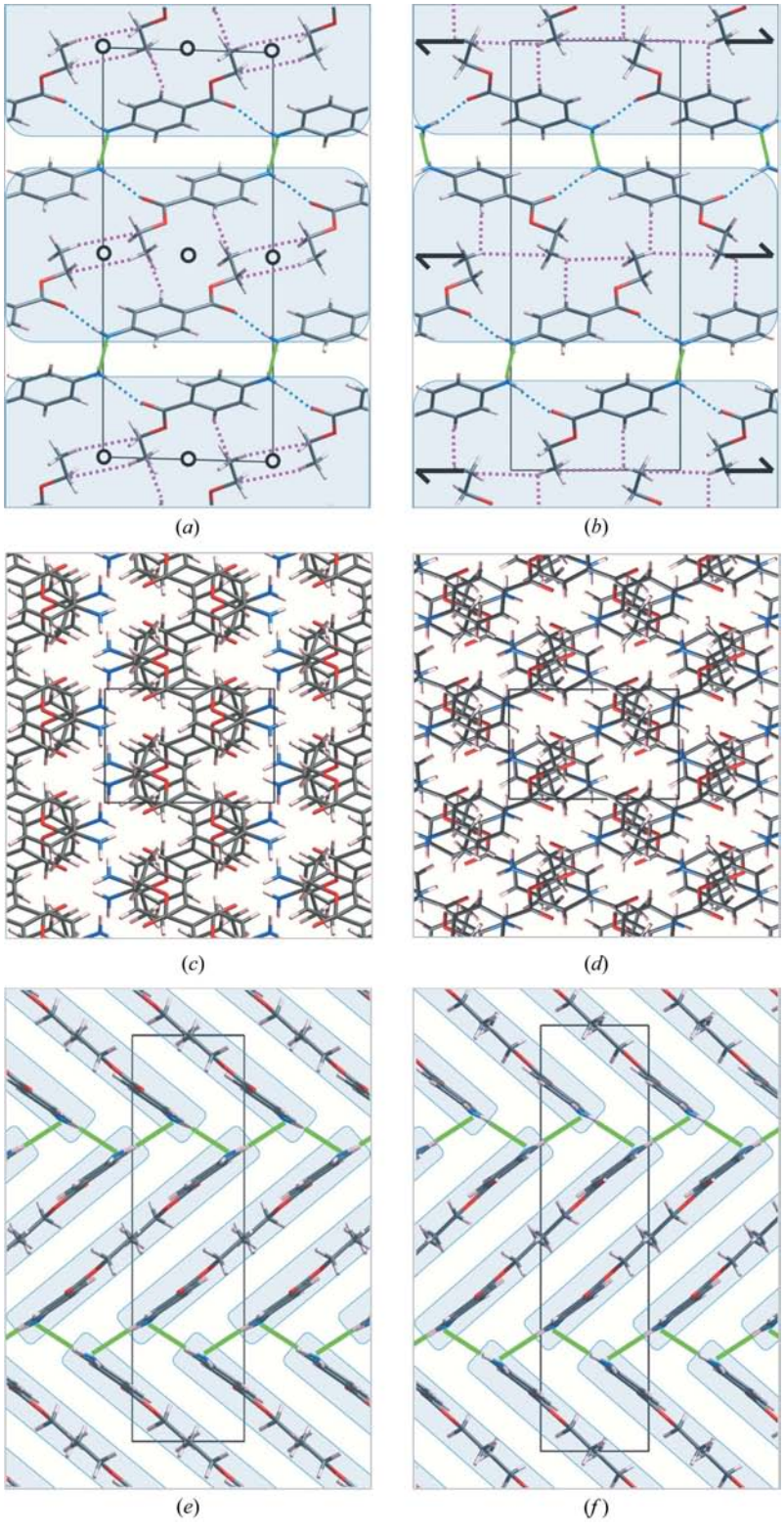

Figure 1
Projections of the structure of the two polymorphs down the three principal axes *a*, *b* and *c*, corresponding to the zero-level diffraction patterns shown in Fig. 2. (*a*) *b* axis form (I); (*b*) *b* axis form (II); (*c*) *c* axis form (I); (*d*) *c* axis form (II); (*e*) *a* axis form (I); (*f*) *a* axis form (II).

Advanced Photon Source synchrotron. The photon energy was 60 keV [λ = 0.2128 (1) Å]. Frames of data were collected using a Mar345 image-plate area detector with a pixel resolution of 0.15 mm. A detector diameter of 300 mm was used, giving frames of size 2000 × 2000 pixels. The sample-to-detector distance was determined using a CeO_2 powder standard as 543.866 mm. The form (I) and form (II) crystals were exposed for 15 s and 10 s, respectively, for each frame and simultaneously rotated through 0.36°. 503 such frames were collected, giving 181.08° of angular coverage. Reciprocal-space sections were reconstructed from the frames using the programs *MarIndex* for indexing of Bragg peaks and *XCAVATE* (Estermann & Steurer, 1998) for reconstruction of specified two-dimensional reciprocal sections. Data from symmetry-related regions were merged. This gave data out to a maximum $\sin\theta/\lambda$ of approximately 0.6109 Å^{-1}.

The data-reduction process to transform the raw data frames to the final reciprocal sections used in the analysis addresses numerous problems associated with the diffuse scattering experiment. These include the presence of air scattering and other forms of parasitic scattering, variation of scale between frames and the presence of different kinds of detector-dependent artefacts. These have been described previously (Welberry *et al.*, 2005). The specific details relevant to the present paper are the same as given in the recent paper by Beasley *et al.* (2008).

2.4. Observed diffuse scattering data

Although full three-dimensional data have been collected the majority of the analysis has been carried out using the three basal plane sections of data for each polymorph. These are shown in Fig. 2. Some particularly strong and interesting features in the patterns are shown in-set as enlargements. Fig. 1 shows projections of the molecular structure corresponding to each of the patterns in Fig. 2. The diffuse scattering has many points of similarity for the two forms, but there are some distinctive differences. We summarize the comparison for each section as follows:

2.4.1. *h0l* sections (Figs. 2*a* and *b*). In this section the scattering of the two polymorphs appears most different because of the different symmetry. Absence of l = odd reflections in form (I) is indicative of the space group *c* glide. The inset figures in Fig. 2(*a*) show the characteristic shape of

the TDS scattering around the Bragg positions. Examples such as the $10\bar{2}$, $\bar{3}0\bar{5}$ and $\bar{4}0\bar{3}$ peaks each have an elongated shape with the long axis normal to a vector from the origin. The strong scattering in the vicinity of the $\bar{7}02$ reflection shows that there is a diffuse band of scattering extending between the Bragg peaks along the *l* row of reflections and normal to **a**. In Fig. 2(*b*) a similar diffuse band of scattering extending between the Bragg peaks along the *l* row of reflections can be seen around the 700 position. The TDS scattering close to Bragg positions in form (II) is rather less pronounced than in form (I). However, the enlarged in-set shows that whereas 200 is elongated vertically 202 is canted inwards.

2.4.2. *hk*0 sections (Figs. 2*c* and *d*). The diffuse scattering observed in this section appears at first sight to be quite similar for the two forms. In both patterns there are (fairly) narrow diffuse bands of scattering extending along vertical rows of Bragg peaks. However, the intensity within these rows is quite different in the two forms. In form (I) the strongest band in the region of 700 has a maximum at the 700 position and diminishes towards the 7, ± 1,0 positions. In form (II) the same band has a minimum at the 700 position and has maxima either side of this. Although much weaker, other *h*00, *h* = odd peaks, such as 500 and 300, show similar separation into two maxima. The *h*00, *h* = even peaks show no such effect, but rather tend to be more extended along *k* than in form (I), *e.g.* see ±2,00. Some rather complex, but quite different, diffuse peak shapes are apparent in the region of ±3,02 in the two polymorphs.

2.4.3. 0*kl* section (Figs. 2*e* and *f*). The diffuse scattering in this section is very strong and highly structured for both polymorphs. The scattering looks practically identical for the two, although there are some small differences; *e.g.* the intensity of the row of diffuse crosses from 00,10 to 00,18. The main features are the sets of elongated diffuse *cigars* that are directed diagonally from top-left to bottom-right and from top-right to bottom-left of the figure. These features show distinct *transverse polarization*. That is to say: those cigars pointing towards the top-left are strongest in the top-right and bottom-left quadrants and are practically absent in the top-left and bottom-right quadrants. Only along, or close to, the two axes do the two sets of cigars intersect to produce the cross-shaped features. In fact, although these features have the appearance of cigars in this section, in three dimensions they are in fact more like oblate spheroids with the minor axis lying within this section and with an aspect ratio of ∼ 4.3:1.

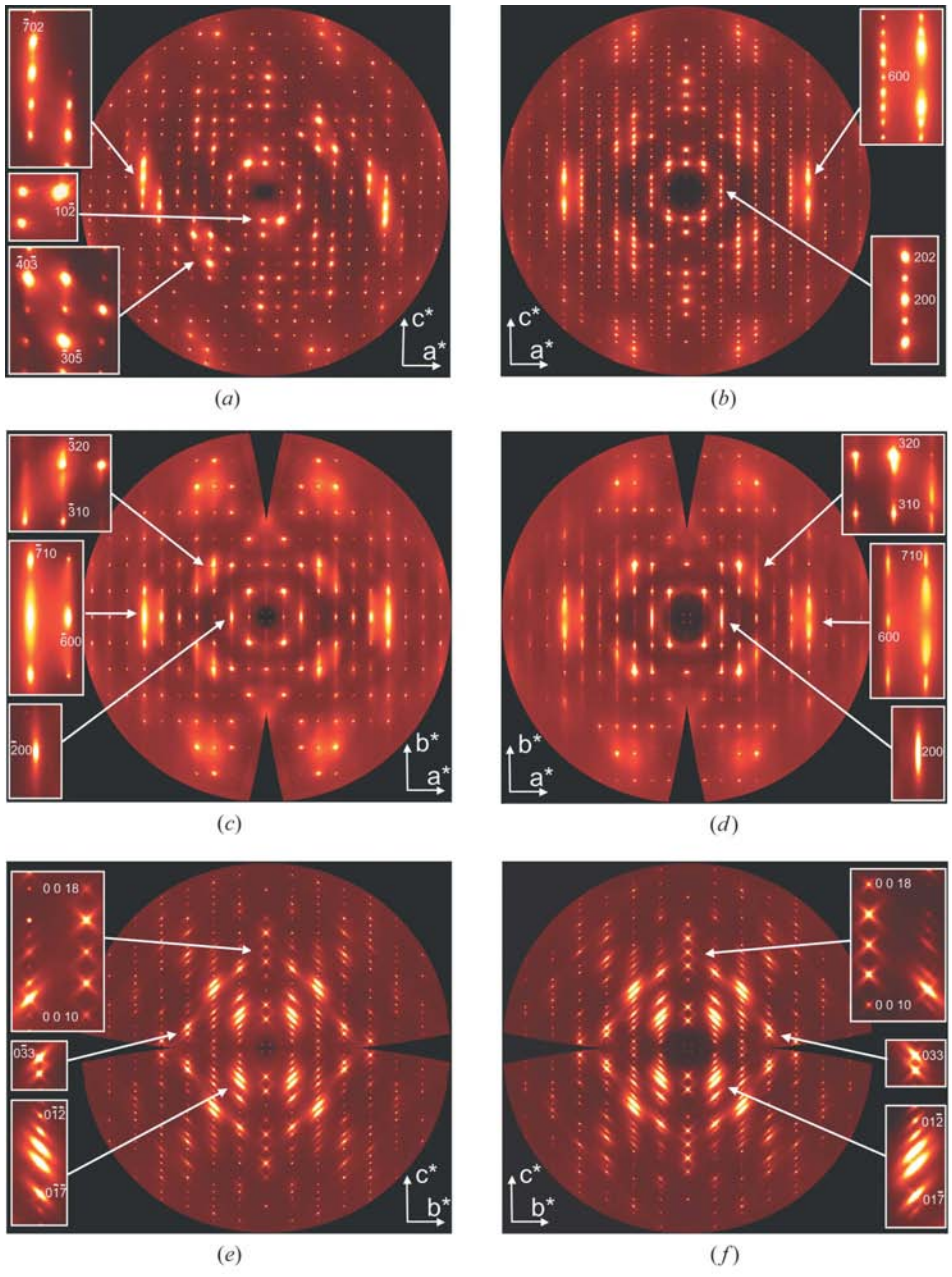

Figure 2
Zero-level sections of the observed diffuse scattering data for the two room-temperature polymorphs of benzocaine. (*a*) *h*0*l* form (I); (*b*) *h*0*l* form (II); (*c*) *hk*0 form (I); (*d*) *hk*0 form (II); (*e*) 0*kl* form (I); (*f*) 0*kl* form (II).

Table 2
The z matrix used to represent the BZC molecule.

Entries i, j and k refer to atom numbers and specify the connectivity of the molecule. Atom $x24$ is a dummy atom. The dihedral angles, L_i, that were allowed to vary have been printed in bold and marked with asterisks.

Atom number	Atom label	i	Bond length (Å)	j	Bond angle (°)	k	Dihedral angle (°)
1	C1	0	0.000	0	0.00	0	0.00
2	C2	1	1.390	0	0.00	0	0.00
3	C3	2	1.371	1	121.39	0	0.00
4	C4	3	1.390	2	120.56	1	−0.02
5	C5	4	1.396	3	118.23	2	−0.69
6	C6	5	1.370	4	120.74	3	0.67
7	C7	1	1.468	6	119.93	2	−179.77
8	O8	7	1.209	1	124.90	6	**3.98***
9	O9	7	1.337	8	122.08	1	178.97
10	C10	9	1.449	7	117.34	8	**0.48***
11	C11	10	1.487	9	107.15	7	**−176.16***
12	N12	4	1.373	5	121.11	3	177.66
13	H13	2	0.928	3	120.52	1	179.51
14	H14	3	0.966	4	119.59	2	−177.14
15	H15	5	0.953	6	122.57	4	−177.38
16	H16	6	0.948	5	119.97	1	−178.33
17	H17	10	0.944	11	115.53	9	117.45
18	H18	10	1.025	17	109.55	11	−129.70
19	H19	11	0.953	10	110.79	18	−172.15
20	H20	11	0.992	19	109.14	10	122.14
21	H21	11	0.993	20	106.86	19	−114.69
22	H22	12	0.864	4	117.57	5	**166.78***
23	H23	12	0.912	22	120.10	4	152.70
24	$x24$	6	1.375	16	178.29	5	−94.80

3. Diffuse scattering analysis

Monte Carlo (MC) computer simulation of a model structure has become a powerful and well accepted technique for aiding the interpretation and analysis of diffuse scattering patterns (Welberry, 2004; Weber *et al.*, 2001; Weber & Bürgi, 2002). In this method a computer model is set-up based on known physical and chemical principles with adjustable parameters describing the basic interatomic or inter- and intramolecular interactions and possible mechanisms for disorder. Diffraction patterns are then calculated from the results of the simulations and these are compared with the observed data. As a result of the comparison adjustments are made to the model parameters and the process is repeated until agreement between observed and calculated patterns is obtained.

In the present case, as in a recent study of *p*-(*N*-methylbenzylidene)-*p*-methylaniline (Beasley *et al.*, 2008), the diffuse scattering is assumed to be purely thermal in origin and consequently the MC models simply comprise sets of harmonic (Hooke's law) springs to represent the intermolecular interactions and torsional springs to provide restoring forces on variable internal dihedral angles.

The MC energy takes the form

$$E = \sum_{\text{all linear springs}} K_i(d - d_0)^2 + \sum_{\text{torsional springs}} L_i(\varphi - \varphi_0)^2. \quad (1)$$

Here d and φ are instantaneous values of the spring lengths and torsion angles, and d_0 and φ_0 the corresponding mean values obtained from the average structure. K_i and L_i are the spring constants which comprise the model parameters that are determined in the process of fitting to the observed data. A sufficient number of MC cycles are performed for the system to attain (or closely approach) equilibrium.

3.1. Monte Carlo model

An MC computer model was constructed for each of the two polymorphs using the atomic coordinates derived from the average structure determinations. A z matrix description of these coordinates was derived so that the complete structures could be defined by the contents of the z matrix, quaternions defining the molecular orientations and sets of translations defining their positions in the unit cell. The same z matrix was used for the analysis of both structures and this is given in Table 2. Molecules were treated as a number of rigid fragments with only the rotations around single bonds providing internal flexibility. The four dihedral angles that were allowed to vary have been marked with asterisks. All other entries in the z matrix were kept constant throughout.

The linear springs, with force constants K_i in (1), that are used to represent the intermolecular interactions, were placed along a carefully selected subset of the large number of atom–atom vectors that typically make up a given intermolecular interaction. This subset of atom–atom interactions comprise the *effective* intermolecular interactions that are used in the simulations. Use of such effective interactions is necessary to reduce the computational task to a tractable level. In choosing these vectors the aim is to reduce the number to a manageable level while retaining a sufficient number to define robustly the separation and mutual orientation of neighbouring molecular fragments. Two or three such atom–atom vectors are usually sufficient for each pair of neighbouring molecular fragments. Provided this criterion is met the actual choice of vectors is less important.

In the present study the sets of vectors used for forms (I) and (II) were chosen to be as similar as possible, with only the vectors across the interface between ribbon pairs being substantially different. (see Figs. 1*a* and *b*). Table 3 lists the vectors that were used in the analysis. In all, 15 unique types of vector were used, each of these requiring the specification of a unique spring constant, K_i. Together with four torsional spring constants, L_i, the total number of parameters determined in each analysis was 19.

3.2. Simulation

The majority of the simulations were carried out using a model crystal comprising $48 \times 48 \times 48$ unit cells. Initial values were assigned to the K_i and L_i force constants and then MC simulation was carried for 2000 MC cycles. One MC cycle is defined as that number of individual MC steps required to visit each molecule once on average. At each MC step a molecule was chosen at random and the variables specifying its conformation (4 dihedral angles), orientation (4 quaternion components) and position (x, y and z coordinates) were subjected to random increments. The system energy was calculated before and after the shift using (1) and the move was accepted or rejected using the normal Metropolis algo-

Table 3
Summary of the interaction vectors used.

Examples given here are for the molecule with symmetry x, y, z. N = neighbour identifier; V = vector type; O = origin atom; C = cell translation of destination molecule with respect to symmetry operated origin molecule; S = symmetry relationship of destination molecule to origin molecule; D = destination atom; L = length of vector; $F1$ = spring constant, K_i, (qualitative); $F2$ = spring constant, K_i, (quantitative); L_1 to L_4 are the torsional force constants.

Polymorph (I)									Polymorph (II)								
N	*V*	*O*	*C*	*S*	*D*	*L*	*F*1	*F*2	*N*	*V*	*O*	*C*	*S*	*D*	*L*	*F*1	*F*2
1	1	H21	000	i	C2	3.008	1.0	1.4 (1)	1	1	H21	000	i	C3	2.943	3.6	1.8 1)
	2	H21	000	i	*x*24	2.824	2.2	2.9 (2)		2	H21	000	i	*x*24	3.879	2.9	1.5 (1)
2	3	H20	110	i	C10	3.191	1.2	1.4 (3)	2	3	H20	010	i	C11	3.313	11.6	5.5 (3)
										4	H20	010	i	H13	2.411	11.6	5.7 (2)
3	4	C11	010	i	H13	2.889	2.0	2.6 (2)									
4	5	C6	000	ii	H15	3.078	1.3	2.0 (1)	3	5	C6	000	ii	H15	3.061	2.7	1.4 (2)
	6	O8	000	ii	H15	2.851	0.7	1.5 (1)		6	O8	000	ii	H15	2.871	2.7	1.5 (1)
5	7	N12	$\bar{1}$00	ii	H23	2.426	2.5	3.5 (1)	4	7	N12	$\bar{1}$00	ii	H23	2.332	4.8	2.4 (1)
6	8	H17	110	iii	N12	3.285	1.3	2.2 (2)	5	8	H17	110	iii	N12	3.295	0.9	0.6 (1)
7	9	O8	100	iii	H14	2.746	3.0	4.4 (2)	6	9	O8	100	iii	H14	2.759	21.6	10.5 (6)
	10	O8	100	iii	H22	2.105	3.5	4.8 (1)		10	O8	100	iii	H22	2.051	21.6	10.4 (2)
8	11	O9	010	iii	C6	3.753	0.4	0.8 (1)	7	11	O9	010	iii	C6	3.756	0.9	0.7 (1)
	12	C2	010	iii	H15	3.195	0.5	1.1 (1)		12	C2	010	iii	H15	3.233	1.1	1.0 (1)
	13	H13	010	iii	C5	3.216	0.5	1.1 (1)		13	H13	010	iii	C5	3.218	1.1	1.0 (1)
	14	H19	010	iii	O8	2.907	0.4	0.9 (1)		14	H19	010	iii	O8	2.993	0.9	0.6 (1)
	15	H19	010	iii	C7	2.900	0.4	0.9 (1)		15	H19	010	iii	C7	2.917	0.9	0.7 (1)
L_1							50	56 (15)	L_1							–	68 (8)
L_2							100	120 (17)	L_2							–	127 (12)
L_3							50	65 (16)	L_3							–	70 (6)
L_4							50	52 (17)	L_4							–	68 (1)

Symmetry codes for polymorph (I): (i) $1-x, 1-y, 1-z$; (ii) $1-x, \frac{1}{2}+y, \frac{1}{2)}-z$; (iii) x, y, z; for polymorph (II): (i) $(1/2)+x, 1-y, 1-z$; (ii) $1-x, \frac{1}{2}+y, \frac{1}{2}-z$; (iii) x, y, z.

rithm (Metropolis *et al.*, 1953) with Boltzmann partition $P = \exp(-\Delta E/k_{\rm B}T)$. The simulation temperature was maintained at a constant value of $T = 1/k_{\rm B}$, where $k_{\rm B}$ is Boltzmann's constant. The force constants used in the simulation are thus measured relative to $k_{\rm B}T$. During the course of the simulation the MC step acceptance/rejection ratio was monitored as a function of the magnitude of each component of the shift vector. As a result of this the magnitudes of the shifts applied in the simulation were adjusted in order that the ratio was maintained at a value close to 1 for each variable.

3.3. Fitting of the model to the observed data

The suitability of the initial choice of springs was first tested by calculating reciprocal-space sections from the simulation coordinates as different values for each force constant were tried. Calculation of diffraction patterns was carried out using the program *DIFFUSE* (Butler & Welberry, 1992). The aim at this stage of the analysis is to see whether the model is capable of producing a correlation structure (and hence a diffraction pattern) displaying all the qualitative features found in the observed patterns. The selection of vectors is a sufficiently flexible process that additional vectors can be added or redundant ones removed quite easily at this stage if the model is found incapable of doing this. As a result of this initial process the sets of 15 vector types (V) defined in Table 3 for the two polymorphs were established and these were used for the remainder of the study. The values for the force constants ($F1$), which gave qualitatively acceptable diffraction patterns during this initial process, were set as a starting point for a more quantitative least-squares fit using an automated refinement procedure (Welberry *et al.*, 1998). The final values ($F2$) of the force constants derived from this fit are thus considered to give the best quantitative fit that the model can provide.

The use of full three-dimensional data in this fitting process is still not computationally feasible and the fit was carried out using only data in the three basal plane sections shown in Fig. 2. However, as a cross-check, other non-zero level sections were calculated from time to time and visual comparison made with the observed data for these sections to ensure the model was consistent with the whole three-dimensional data. In all 21 795 data pixels were used in the fit for form (I) and 30 522 for form (II).

4. Results

4.1. Calculated diffraction patterns

Fig. 3 shows calculated diffraction patterns for the three basal plane reciprocal sections for both polymorphs (I) and (II); *cf.* the corresponding observed sections shown in Fig. 2. Shown in-set are enlarged small regions of the patterns corresponding to those also shown in Fig. 2. The observed and calculated patterns are seen to be in very good agreement, with all of the detailed features of the patterns well reproduced. This is borne out by the quantitative agreement factors that were achieved.

The agreement factor, $R = \left[\sum \omega(\Delta I)^2 / \sum \omega I_{\rm obs}^2\right]^{1/2}$, was 0.126 for form (I) and 0.172 for form (II), calculated on a pixel-

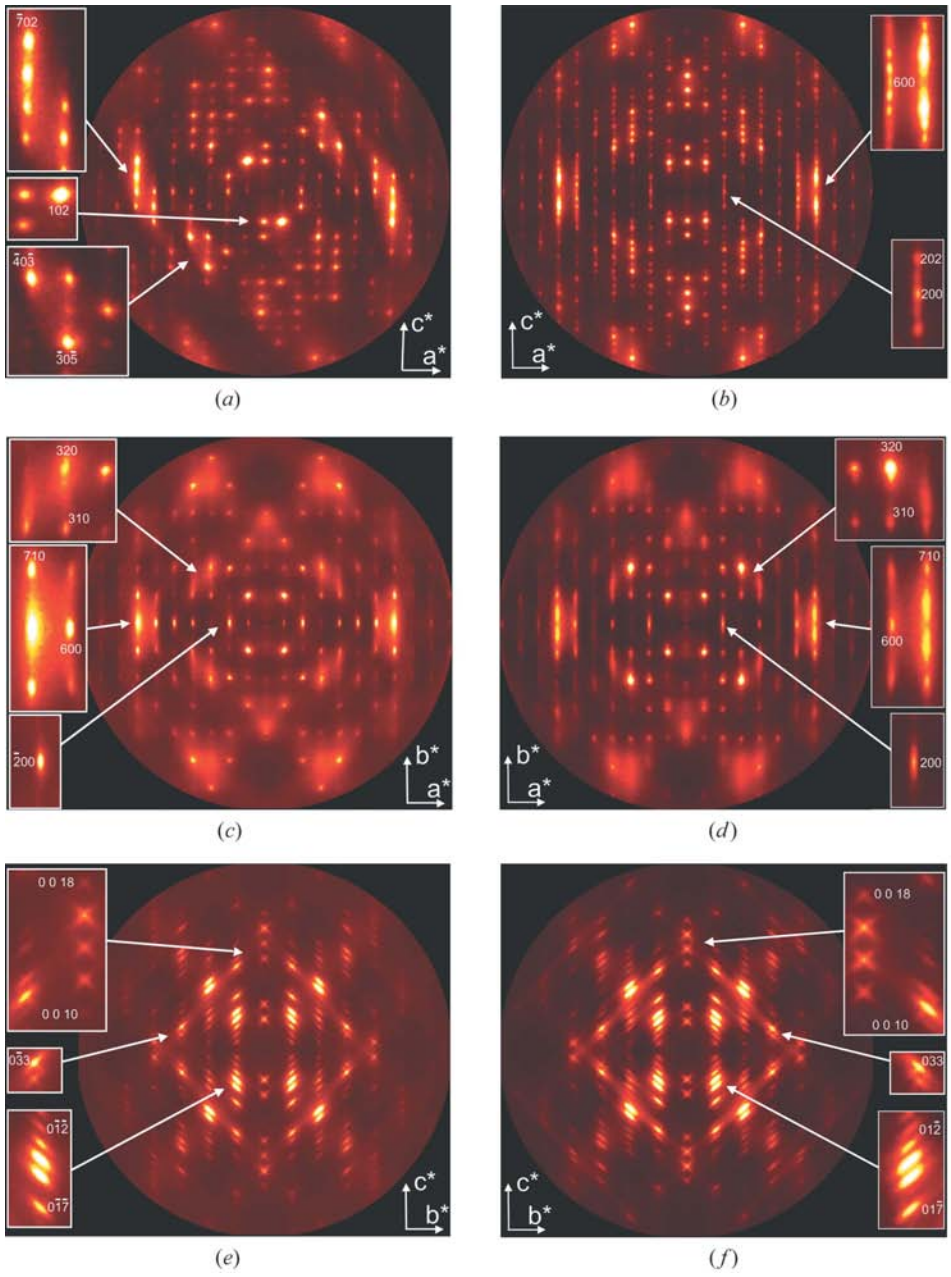

Figure 3
Zero-level sections of the diffuse scattering for the two room-temperature polymorphs of benzocaine calculated from the MC simulations. (*a*) *h*0*l* form (I); (*b*) *h*0*l* form (II); (*c*) *hk*0 form (I); (*d*) *hk*0 form (II); (*e*) 0*kl* form (I); (*f*) 0*kl* form (II); *cf.* the observed data in Fig. 2.

by-pixel comparison over selected regions of the three reciprocal sections of data shown in Fig. 2. In total 21 795 datapoints were used for form (I) and 30 522 for form (II), with weights given by $\omega = 1/I_{\rm obs}$.

4.2. Displacement correlations.

A useful way of interrogating the final model coordinates, in order to gain an appreciation of how the molecules are behaving, is to display the way in which the displacements of neighbouring molecules (or parts thereof) are correlated with each other. This can be done by plotting so-called *peanut*[1] or correlation diagrams, an example of which is shown in Fig. 4(*a*). If X_A is the component of the displacement of molecule A in a direction defined by an angle φ from some reference direction and X_B is the component of the displacement of molecule B in the same direction, then the correlation coefficient, C_φ, for these displacements is given by

$$C_\varphi = \frac{\langle X_A X_B \rangle}{\left(\langle X_A^2 \rangle \langle X_B^2 \rangle\right)^{1/2}}.$$

4.2.1. Correlations in the *bc* plane. Fig. 4(*b*) shows plots of C_φ for displacements of the centre of mass of a reference molecule with displacements of successively distant molecules related by cell translations in the *b* (horizontal) and *c* directions (vertical). Fig. 4(*c*) shows a projection of the structure in which some of these intermolecular correlation vectors have been marked. Each of the small squares in Fig. 4(*b*) corresponds to a range of ± 0.2 in the value of the correlation coefficients. The correlation values for the nearest neighbours, [010] and [0$\bar{1}$0], exceed this range, while for molecules with a component of two translations along *c* the correlation values are generally very small.

What is most significant here is that for vectors at approximately 45° to the *b* axis, typified by those to [0$\bar{3}$1] and [031], the peanuts are highly anisotropic with the major correlation direction pointing along the vector and with virtually zero lateral correlation. This is true both for [0$\bar{3}$1], where the molecular planes of the origin and target molecule are normal to the connecting vector, and for [031], where the molecular

[1] It should be noted that the word *peanut* has also been used to describe atomic displacement parameters (ADPs) in the context of the analysis of Bragg scattering from molecular crystals (Hummel *et al.*, 1990; Trueblood *et al.*, 1996).

planes of the origin and target molecule are parallel to the vector. It is these strong longitudinal correlations that give rise to the narrow *cigar*-shaped features observed in Figs. 2(*e*) and (*f*). Even the peanuts for [0$\bar{6}$2] and [062] (not shown) are significantly non-zero, indicating that the displacement of any given molecule affects neighbours at distances of 50 Å or more.

The array of correlation diagrams like that shown in Fig. 4(*b*) is like a fingerprint that describes the molecular motions in a crystal when viewed down a particular axis. We have found such diagrams very useful for obtaining insight into the way molecules move relative to each other and for comparing the behaviour of different systems. Fig. 4(*a*) was computed from the MC simulation of polymorph (I). For polymorph (II) the corresponding diagram is virtually identical, indicating that when viewed from this direction the two polymorphs are very similar.

4.2.2. Correlations in the *ab* plane. Figs. 5(*a*) and (*b*) show similar plots to Fig. 4(*a*). In this case the plots are of correlations within a single *ab* molecular layer normal to *c* for polymorphs (I) and (II). These plots indicate significant differences between the two polymorphs, although both are dominated by the very strong longitudinal correlations along the hydrogen-bonded chains of molecules running in the *a* direction. This correlation arises as a result of the strong

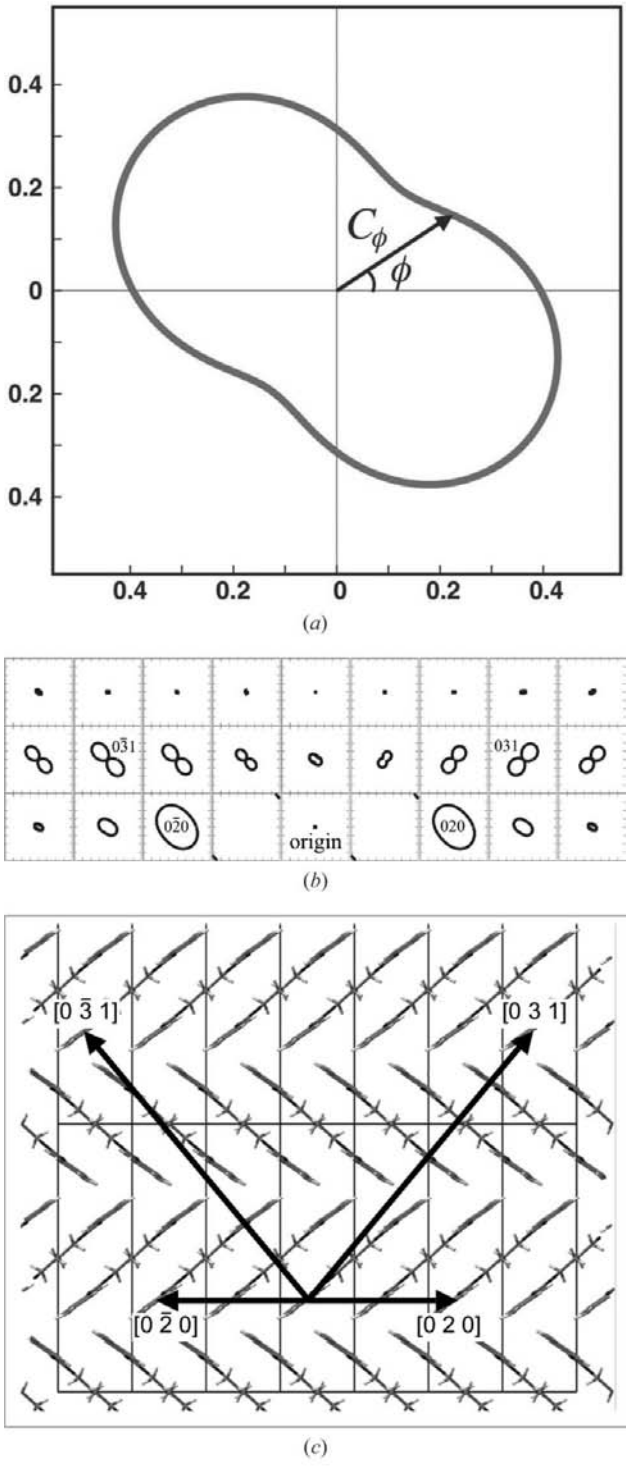

Figure 4
(*a*) An example correlation diagram showing labelling. (*b*) An array of correlation diagrams for displacements in the *bc* plane of polymorph (I). (*c*) A projection of the structure viewed down *a* showing examples of the vectors for which correlations are shown in (*b*). See text for details.

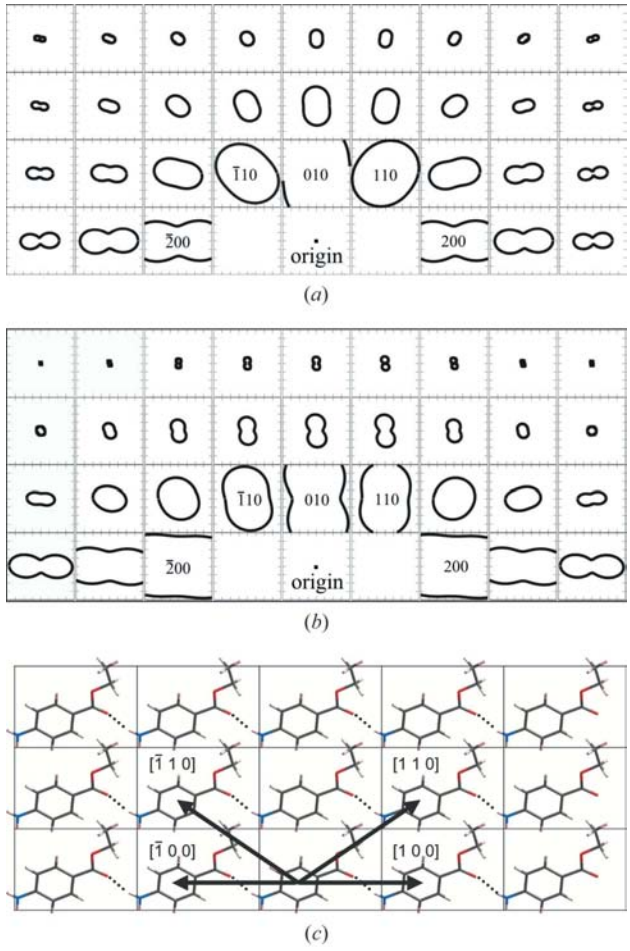

Figure 5
(*a*) Correlation diagrams for displacements within a single *ab* molecular plane of polymorph (I). (*b*) Corresponding diagrams for polymorph (II). (*c*) A single molecular layer of the structure viewed down *c* showing examples of the vectors for which correlations are shown in (*a*) and (*b*). See text for details.

spring constants along vectors V = 9 and 10 in Table 3, that were obtained in the MC model refinements. This row of strong longitudinal correlations indicates that the molecular chains tend to slide along a as relatively rigid units. This tendency is strong for polymorph (I) but is even stronger for polymorph (II). It is these correlated chains of molecules that give rise to the observed sheets of diffuse scattering which occur normal to a^* and which may be seen in Figs. 2(*c*) and (*d*).

The correlations in the next row (k = 1) of diagrams in Figs. 5(*a*) and (*b*) show how the motions of neighbouring chains (one b translation away) behave rather differently in the two structures. This is most noticeable in the plots for [$\bar{1}$10], [010] and [110]. For polymorph (II) these correlation diagrams are rather narrower in the a direction, indicating that there is less tendency for the sliding of one chain to drag the next chain along with it.

It should be remembered, however, that the molecules in these correlated chains are inclined to the ab plane and are in fact more intimately associated with the chains in the next molecular layer down when viewed down c. Together these pairs of chains form the molecular ribbons which are highlighted by the blue shading in Figs. 1(*a*), (*b*), (*e*) and (*f*). These ribbon pairs are held together by springs along vectors V = 3 and 4 in Table 3. Again it is seen that these forces are stronger in polymorph (II) than in polymorph (I). This indicates that the sliding motion of the molecular chains along a tends to occur as ribbon pairs in polymorph (II) more strongly than in polymorph (I).

4.3. Symmetry of ribbon pairs

As can be seen from Figs. 1(*a*) and (*b*) the ribbon pairs discussed above have, on average, different symmetries. For polymorph (I) the two chains comprising the ribbon pair are related by a centre of symmetry, whereas for polymorph (II) they are related by a 2_1 screw. On the local scale, however, this average symmetry does not need to be obeyed. For example, if the forces connecting the two members of a given ribbon pair are weak then it might be expected that the motion of the two chains will not be strongly coupled – *i.e.* they will tend to slide independently – and at a given instant the average symmetry will be broken on the local scale. On the other hand, if the coupling between the two is strong then the two chains will tend to move together as a unit and the average symmetry will be preserved on the local scale. This has an important effect on the diffuse diffraction pattern, particularly for polymorph (II).

For polymorph (II) the 2_1 screw axis parallel to the a axis gives rise to the systematic absence of h00 Bragg peaks with h = odd. If the chains of molecules tend to move independently then the planes of diffuse scattering which occur normal to a^* will not show any systematic extinction effects. On the other hand, if the motions tend to preserve the 2_1 screw symmetry at the local level then the same extinction rules should apply to the diffuse scattering as for the Bragg scattering. The separation of the strong diffuse band of scattering in the region of the 700 reciprocal point in Fig. 2(*d*) into two distinct peaks with a minimum at the exact 700 position is a direct consequence of this. This feature is reproduced in the MC model as a direct consequence of the strong spring constants V = 3 and 4 in Table 3. If the magnitude of these two spring constants is reduced the two peaks gradually merge into a single peak centred on 700 and this diffuse feature then appears very similar to that for polymorph (I).

4.4. Summary of results

The models that have been developed to describe the two polymorphs both give good agreement with the observed diffuse scattering data. Both models show that a key feature of the molecular motions within the crystals is a tendency for hydrogen-bonded chains of molecules running along a to slide back and forth in this direction as relatively rigid units. This sliding motion of one chain is strongly correlated to that of the neighbouring chain with which it forms a ribbon pair (see Fig. 1). The refined force-constant parameters indicate that the effect is more pronounced for polymorph (II). The sliding motion is much less correlated between different ribbon pairs. For displacements perpendicular to the ribbon pairs the two polymorphs behave virtually identically with strong longitudinal correlations extending out to large distances in directions approximately $\pm 45^\circ$ to the b axis.

The models that have been used in this paper are thermal in nature with the effective intermolecular forces provided by purely harmonic springs. Despite the generally good fit to the data for both polymorphs that for polymorph (II) is significantly less good, suggesting that something is still lacking in the model for this system. In particular, there is one feature of the diffraction pattern of polymorph (II) that the model has not been able to fit very well. This is the elongated diffuse peak that occurs in the region of the 200 Bragg position (see Fig. 2*d* inset). Despite extensive exploration of the parameter space using the chosen set of springs as well as invesigating the effect of different sets of springs it has not been possible to obtain a model simulation to produce enough intensity in this position nor to give it a sufficiently elongated profile.

4.5. Phase transition in polymorph (II)

For purely thermal diffuse scattering the diffuse intensity in the close proximity of a Bragg position tends to be proportional to the Bragg peak intensity itself, *i.e.* it is dependent on the structure factor of the average structure. Since the MC model is set up using the coordinates from the average structure, which itself was obtained from the Bragg intensities, this implies that to account for the extra intensity in the region of 200 some alternative mechanism needs to be found. One possibility is that there might be some kind of static disorder in which molecules take up alternative positions or conformations (while maintaining the observed *average* structure). In this case the diffuse intensity includes contributions which are proportional to the difference of structure factors of the two components. A similar effect would also be obtained if this kind of binary disorder were dynamic – as would occur for example if there were anharmonic effects involving double-well potentials. If such a situation were the case then it might

be supposed that, on cooling, the crystal would undergo a phase transition. For this reason low-temperature experiments were undertaken and, as a result, it was found that polymorph (II) does undergo a phase transition to a new polymorph [polymorph (III); see Table 1] while polymorph (I) does not. A study of this phase transition as well as a full description of the average structure of polymorph (III) will be the subject of future papers. For the present purposes we simply show the relationship of this new phase to the room-temperature polymorphs (I) and (II).

Fig. 6(*a*) shows plots viewed down *c* of a single molecular layer in polymorph (II) alongside a corresponding molecular layer in polymorph (III). It is seen that both structures are comprised of virtually identical hydrogen-bonded chains running along *a*. However, while in polymorph (II) these chains are related by translational symmetry along *b*, for polymorph (III) they occur in pairs and this results in a doubling of the cell along *b*. The interactions within one of the pairs is very similar to those in polymorph (II), but between pairs the interface is quite different. To emphasize this point blue and orange intermolecular vectors have been drawn on the two diagrams. For polymorph (II) these two types of vector are identical while for polymorph (III) they are quite different.

Fig. 6(*b*) shows a part of the *hk*0 section of the diffraction patterns for the three polymorphs. The pattern for polymorph (III) was constructed from the frames of data used for collecting Bragg intensities on a conventional laboratory source and so is not of the same quality as the patterns for polymorphs (I) and (II). These data were obtained when a crystal of polymorph (II) was cooled to 150 K and the patterns clearly show that two twinned orientations of the polymorph (III) cell (see Table 1) are present.

Two features of the pattern are of particular interest, and these have been indicated by arrows in the figure. In the region close to the original 200 Bragg position there is now a pair of strong Bragg peaks that are positioned either end of where the elongated diffuse peak occurs in the polymorph (II) pattern. Similarly in the region close to the original 700 Bragg position there are now two pairs of Bragg peaks with diffuse streaks linking them. This motif clearly resembles the diffuse distribution in the polymorph (II) pattern where the diffuse peak around 700 is bimodal. These two observations strongly suggest that the structure that has emerged from the phase transition was being reflected in the dynamic behaviour of the structure in the higher temperature polymorph (II) phase.

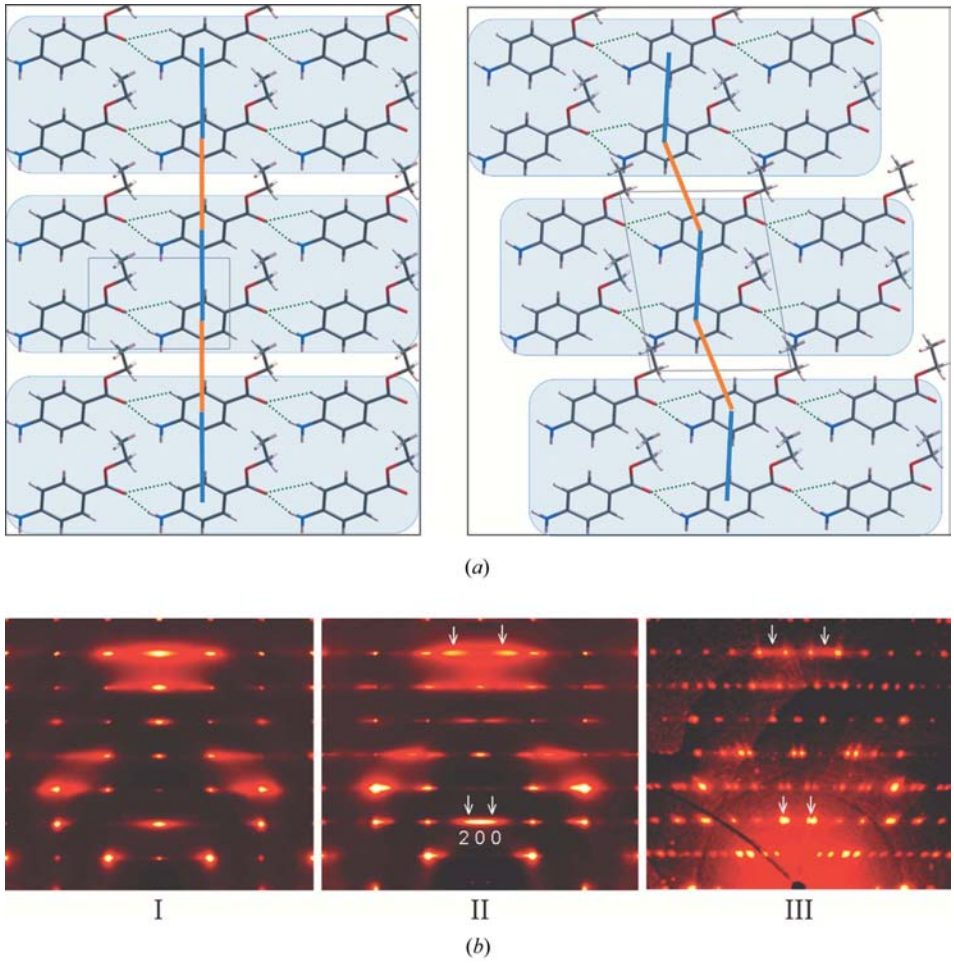

Figure 6
(*a*) A view of a single molecular layer normal to *c* of the structures of polymorph (II) (left) and polymorph (III) (right). Both show chains of hydrogen-bonded molecules running horizontally in the *a* direction. For (II) the chains are all related by a simple *b* cell translation, but for (III) the chains occur in pairs and these are successively shifted to the right. (*b*) A small region of the *hk*0 section of the diffraction patterns of the three polymorphs (I), (II) and (III). Note these diffraction patterns are displayed with a^* vertical and b^* horizontal in order to aid comparison. The features indicated by arrows are referred to in the text.

5. Conclusion

In this paper we have described simple MC models that reproduce in detail the diffuse diffraction patterns that have been observed for the two room-temperature polymorphs of benzocaine. The models use a restricted set of linear harmonic springs to provide effective intermolecular interactions and torsional springs on dihedral angles for intramolecular interactions. 15 linear spring constants K_i and four torsional constants L_i were the only adjustable parameters used in fitting the models to selected regions from the full three-dimensional data that were

recorded. The fitted data were restricted to the three basal plane sections *h*0*l*, *hk*0 and 0*kl* but as a cross-check other sections were also calculated. For polymorph (I) a residual $R = \left[\sum \omega(\Delta I)^2 / \sum \omega I_{\rm obs}^2\right]^{1/2}$ of 0.126 was obtained for a pixel-by-pixel comparison over the selected regions of data which comprised in total 21 795 points. For polymorph (II) the value of R obtained was 0.172 for 30 522 points. For both analyses weights, $\omega = 1/I_{\rm obs}$, were used.

The two analyses were carried out using models that were very similar and which involved fitting the same number of force constant parameters in each case. Each analysis, on its own, resulted in a fit to the observed data which, compared with the levels of accuracy achieved in previous similar analyses, would have been deemed very satisfactory. However, the quantitative comparison between the two revealed that the fit for the polymorph (I) data was significantly better than that for polymorph (II). It was thus inferred that the purely harmonic spring model was inadequate to fully account for the observed data in polymorph (II), suggesting that a disordered or anharmonic model might be required and that the discrepancies might be precursors of an incipient phase transition. As a result of this, low-temperature experiments were carried out and it was discovered that polymorph (II) does undergo a phase transition to a previously unknown form, polymorph (III), which is twinned monoclinic (see Table 1). Diffraction patterns of this new form show enhanced scattering in regions where the polymorph (II) patterns fitted least well, suggesting that a model possessing some of the structural characteristics of this new form could provide a better fit to the data. Further work is in progress to investigate this possibility.

The study as a whole has added further weight to the premise that diffuse scattering contains a wealth of information over and above that obtainable from Bragg scattering and this can provide meaningful insights into the behaviour of molecules in polymorphic systems. The difficulties inherent in structure prediction of flexible molecular systems (Day *et al.*, 2005) show that the study of such systems is far from simple, and it is hoped that the insights that diffuse scattering provides can inform the development of more reliable methods of prediction for these important classes of molecular materials, including molecules of industrial and medical significance.

The support of the Australian Research Council, the Australian Partnership for Advanced Computing and the Australian Synchrotron Research Program are gratefully acknowledged. DJG gratefully acknowledges the support of the Australian Institute of Nuclear Science and Engineering. The authors thank Dr Tony Willis of the Research School of Chemistry for assistance with the collection of the Bragg data and Professor A. D. Rae for helpful discussions. Use of the Advanced Photon Source was supported by the US Department of Energy, Office of Science, Office of Basic Energy Sciences, under Contract No. DE-AC02-06CH11357.

References

Beasley, A. G., Welberry, T. R., Goossens, D. J. & Heerdegen, A. P. (2008). *Acta Cryst.* B**64**, 633–643.
Bernstein, J. (2002). *Polymorphism in Molecular Crystals.* IUCr Monographs on Crystallography. Oxford University Press.
Butler, B. D. & Welberry, T. R. (1992). *J. Appl. Cryst.* **25**, 391–399.
Chan, E. J., Rae, A. D. & Welberry, T. R. (2009). *Acta Cryst.* Submitted.
Day, G. M. *et al.* (2005). *Acta Cryst.* B**61**, 511–527.
Estermann, M. A. & Steurer, W. (1998). *Phase Transitions*, **67**, 165–195.
Gruno, M., Wulff, H. & Pflegel, P. (1993). *Pharmazie*, **48**, 834–837.
Hummel, W., Raselli, A. & Bürgi, H.-B. (1990). *Acta Cryst.* B**46**, 683–692.
Knapman, K. (2000). *Mod. Drug Discovery*, **3**, 53–54.
Lynch, D. E. & McClenaghan, I. (2002). *Acta Cryst.* E**58**, o708–o709.
Metropolis, N., Rosenbluth, A. W., Rosenbluth, M. N., Teller, A. H. & Teller, E. (1953). *J. Chem. Phys.* **21**, 1087–1092.
Schmidt, A. C. (2005). *Int. J. Pharm.* **298**, 186–197.
Sinha, B. K. & Pattabhi, V. (1987). *Proc. Indian Acad. Sci. Chem. Sci.* **98**, 229–234.
Trueblood, K. N., Bürgi, H.-B., Burzlaff, H., Dunitz, J. D., Gramaccioli, C. M., Schulz, H. H., Shmueli, U. & Abrahams, S. C. (1996). *Acta Cryst.* A**52**, 770–781.
Weber, T. & Bürgi, H.-B. (2002). *Acta Cryst.* A**58**, 526–540.
Weber, T., Estermann, M. A. & Bürgi, H.-B. (2001). *Acta Cryst.* **57**, 579–590.
Welberry, T. R. (2001). *Acta Cryst.* A**57**, 244–255.
Welberry, T. R. (2004). *Diffuse X-ray Scattering and Models of Disorder.* IUCr Monographs on Crystallography. Oxford University Press.
Welberry, T. R. & Butler, B. D. (1994). *J. Appl. Cryst.* **27**, 205–231.
Welberry, T. R., Goossens, D. J., Edwards, A. J. & David, W. I. F. (2001). *Acta Cryst.* A**57**, 101–109.
Welberry, T. R., Goossens, D. J., Heerdegen, A. P. & Lee, P. L. (2005). *Z. Kristallogr.* **222**, 1052–1058.
Welberry, T. R., Proffen, T. & Bown, M. (1998). *Acta Cryst.* A**54**, 661–674.